Solid Freeform Fabrication 2022: Proceedings of the 33rd Annual International Solid Freeform Fabrication Symposium – An Additive Manufacturing Conference
Reviewed Paper

In-Situ Infrared Thermographic Measurement of Powder Properties in Laser Powder Bed Fusion

Tao Liu[1], Edward C. Kinzel[2], Ming C. Leu[1]
[1]Mechanical and Aerospace Engineering Department, Missouri University of Science and Technology, Rolla, MO 65409, USA
[2]Aerospace and Mechanical Engineering Department, University of Notre Dame, Notre Dame, IN 46556, USA

Abstract

The laser powder-bed fusion (LPBF) process is strongly influenced by the characteristics of the powder layer, including its thickness and thermal transport properties. This paper presents an investigation of in-situ characterization of the powder layer using active infrared thermography. The printing laser beam is diffused and illuminates onto the powder bed's top surface in various frequencies. A long-wavelength thermal camera monitors the surface temperature history. Insight is provided by a one-dimensional thermal model of the process, which shows the frequency dependence of the surface temperature amplitude and phase on the powder layer thickness and thermal properties. An experiment demonstrates the validity of this model and shows its potential for measuring local powder properties in-situ.

1. Introduction

The laser powder-bed fusion (LPBF) process has potential advantages for manufacturing products with higher dimensional accuracy and complex geometry [1]. In order to improve the quality of the printed products, in-situ inspection techniques have been widely used to study the effects of process parameters such as laser power and scan speed [2,3]. Although having attracted less attention, powder layer properties also affect the printing process and part quality significantly. For example, powder layer thickness influences the porosity [4,5], microhardness [6,7], surface roughness [8], strength, and elasticity [9,10] of the final part. The powder bed also acts as a support for overhang and other complex structures. The surface qualities of these structures are limited by the thermal properties of the powder bed. In order to improve the finish and accuracy of the surface, the laser process parameters need to be optimized based on the knowledge of the local powder's thermal conductivity [11].

The powder layer thickness can be monitored by using high-resolution optical imaging [12], optical coherence tomography (OCT) [13] or fringe projection [14]. The laser displacement approach has also been used to measure the local powder thickness [15]. However, these methods can only capture information about the powder bed surface profile. The thermal conductivity of metal powders has been studied by using ex-situ hot wire [11], ex-situ laser flash [16], and in-situ reflectance measurement [17]. These techniques cannot obtain the powder geometry in-situ. It is much more convenient to measure the powder's layer thickness and thermal properties at the same time.

Infrared thermography (IRT) is one of the nondestructive testing (NDT) techniques using the diffusion of heat through a material to evaluate the subsurface cracks or defects and coating

thicknesses [18]. Compared with other NDTs like hammer sounding and microwave radar, IRT has drawn more attention due to its advantages of real-time, contactless and wide-area measurements [19]. By using IRT, both thickness [20] and thermal properties [21] can be measured. There are two different types of IRT including passive and active, which are based on different types of heating sources [22]. The passive IRT was used to measure the powder layer's thickness in our previous work [23], which used the printed part beneath the powder layer as the heating source.

This paper investigates an active IRT based technique to estimate the powder layer's thickness and thermal properties. The printing laser serves as the heating source. By controlling the printing laser exposure time and hatch pattern, the powder layer is heated by absorbing the laser's periodic illumination with respect to time. The temperature history of the powder's top surface is observed with a long wavelength infrared (LWIR) camera. After analysis of the temperature history, the transient thermal response is correlated with the powder thickness and thermal properties. A validating experiment is conducted for this correlation. A heat transfer model (1D) is established to compare analytical predictions with experimental results.

2. Experimental Setup

Figure 1 illustrates the experimental setup with a long-wavelength infrared (LWIR) camera (FLIR A655sc) integrated with a commercial LPBF machine (Renishaw AM250). A ZnSe window on the chamber allows the LWIR camera to observe the build plate from 15° off-normal. The LWIR camera has the resolution of 640×480 pixels, corresponding to a spatial resolution of 325 µm for this configuration. The spectral range of this LWIR camera is 7.5-14.0 µm. The noise-equivalent temperature difference (NETD) is 30 mK and the frame rate is 200 Hz (with zoom in 640×120 pixels). The camera reports the temperature of the scene assuming an emissivity of 0.95 (gray-body approximation), which is not corrected for transmission through the window. After transferring the temperature from time domain to frequency domain, the amplitude can be separated from the phase information. This removes requirements for emissivity information and non-uniformity calibrations, significantly simplifying the instrumentation. The laser is expanded by an optical diffuser (DG100×100-220, Thorlabs) and fixed 30 cm above the surface of the powder bed.

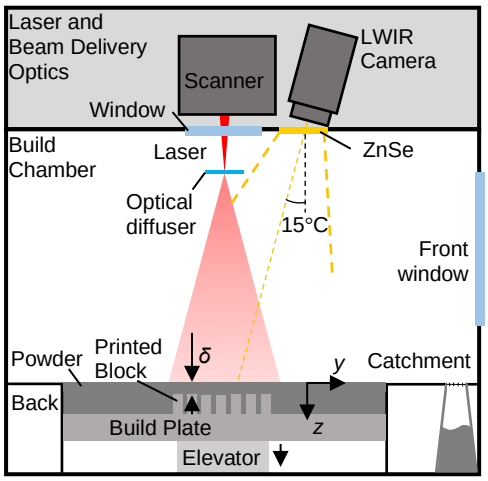

Figure. 1. Illustration of the LPBF experimental setup including a LWIR camera.

In order to collect the temperature histories for various known powder thicknesses, simple gage specimens are printed with the Renishaw AM250. They consist of 7 cuboid blocks (5×5 mm^2) with different elevations, h, from a printed datum plane. After the specimen is printed, the wiper (recoater) then spreads new powder over the build plate including the specimen. This gives a powder layer thickness that varies spatially with the height of the individual blocks. The powder layer thickness is $\delta=h_0-h$, where h_0 is the height above the datum of the build plane. In this experiment h_0=1 cm so that the highest specimen has δ=100 µm of powder above it. The heights of the gage specimens and corresponding powder thicknesses are listed in Table 1. The temperature of the build plate is constant at 50 °C.

Table 1 The heights of seven different blocks and corresponding powder thicknesses

n	h [mm]	δ [µm]
1	9.90	100
2	9.85	150
3	9.80	200
4	9.75	250
5	9.70	300
6	9.65	350
7	9.60	400

Figure 2 shows the temperature history of a single pixel for the 200 W laser of AM250 illuminating the sample 100 times at the frequency of 0.25 Hz, using 304L stainless steel powder with different layer thicknesses. The powder used has particle diameters ranging between 15 and 40 µm, with a mean diameter 25 µm. The laser illuminating has a square wave. As shown in Fig. 2, from t ≈ 8 s the temperature of the powder starts to increase from around 50 °C and oscillates at 0.25 Hz with the laser's periodic illumination. The laser is turned off after 100 cycles at t ≈ 408 s, and then the powder temperature begins to cool down.

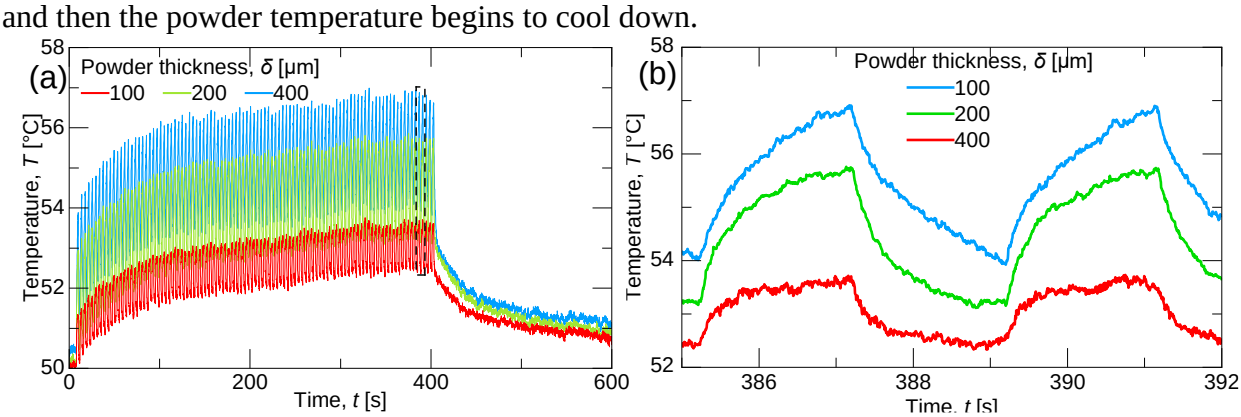

Figure. 2. Temperature history of a single pixel for (a) a periodic heating process at 0.25 Hz for 100 times and the dash marked portion is shown in (b).

The periodic temperature history can be fitted with a Fourier series by using linear least square regression as follows:

$$
\begin{aligned}
T &= C + t^D + \sum_{n=1}^{N}\left[T_n \cos\left(2\pi f_n t + \varphi_n\right)\right] \\
&= C + t^D + \sum_{n=1}^{N}\left[\alpha_n \cos\left(2\pi f_n t\right) - \beta_n \cos\left(2\pi f_n t\right)\right] \\
f_n &= \left(2n-1\right) f_1
\end{aligned}
\tag{1}
$$

where T is temperature, t is time, T_n and φ_n are the amplitude and phase of the temperature at frequency f_n. Since the laser heating source has a square wave, the frequency f_n is an odd integer multiplying the fundamental frequency f_1 (e.g., 0.25 Hz). t^D is the power function of t with index D. C, D, α_n, and β_n are fitting coefficients. Then the amplitude and phase of the temperature are

$$
\begin{aligned}
\left|T_n\right| &= \sqrt{\alpha_n^2 + \beta_n^2} \\
\varphi_n &= tan^{-1}\left(\frac{\beta_n}{\alpha_n}\right)
\end{aligned}
\tag{2}
$$

An example fitting result is shown in Fig. 3. After fitting the temperature history by using Eq. 1, the values of C, D, α_n, and β_n are determined. Then the phases for different powder thicknesses at various frequencies can be obtained.

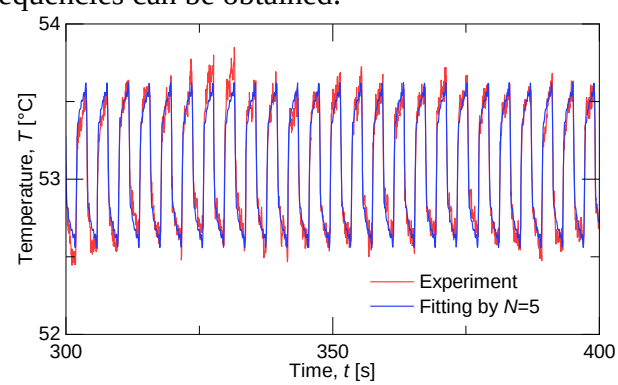

Figure. 3. Comparison between experimental data with the fitting result for δ = 100 μm.

Figure 4 shows the phases for different powder thicknesses at the first (fundamental) frequency of the square wave, f_1 = 0.25 Hz. It is obvious that the phase can be correlated to powder thickness with a monotone relationship: the larger the powder thickness, the smaller the phase angle. This relationship can be used to predict the powder thickness using the phase difference between the periodic laser heating and the measured surface temperature.

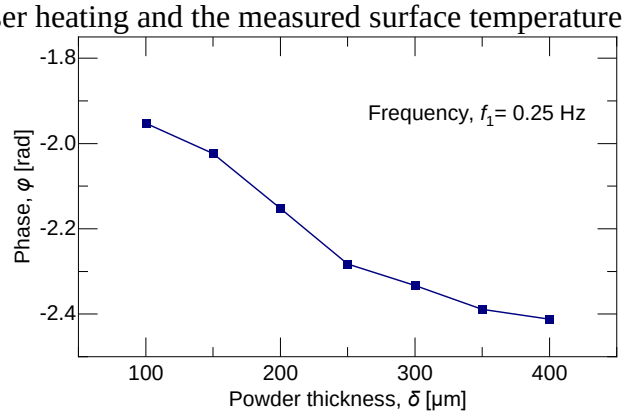

Figure. 4. Experimental correlation between phase and powder thickness with the fundamental frequency f_1 = 0.25 Hz.

3. 1D Heat Transfer Model and Finite Difference Solution

The powder surface temperature history can be predicted by modeling the thermal diffusion through the powder from the periodic laser heating. Since the thickness of powder layer is much smaller than the lateral dimensions of the blocks (5 mm), it is reasonable to model the problem as 1D heat transfer in z-direction. The powder is evaluated as a continuous medium, with its thermal properties being temperature independent. A schematic diagram of this model is shown in Fig. 5(a), which shows a powder layer of thickness δ is in contact with a printed block. A diffused laser with illumination heat flux q_{laser} in a square wave is emitted on the top surface of the powder, and it is assumed that the heat from the laser is completely absorbed by the powder (100% absorption). A convection boundary condition is applied with h = 15 W/m^{2}K. The printed block is in perfect contact with the build plate, whose temperature is constant at 50 °C. The environment temperature is 30 °C.

The heat transfer problem as described is governed by the following equation:

$$\frac{\partial T}{\partial t} = \frac{k_i}{\rho_i c_i}\frac{\partial^2 T}{\partial z^2} \tag{3}$$

with the boundary conditions

$$\begin{aligned} &k_p \left.\frac{\partial T}{\partial z}\right|_{z=0} = h\left[T\left(z=0,t\right)-T_\infty\right]-q_{laser} \\ &T_\infty = 30°C \\ &T\left(z=L,t\right)=50°C \end{aligned} \tag{4}$$

and the initial condition

$$T\left(z,t=0\right)=50°C \tag{5}$$

The thermal properties in Eq. (3) depend on the form of material, which may be either powder or printed block (denoted by the subscript, i, which is p for powder and b for block). k, ρ and c are the effective thermal conductivity, density and specific heat of the material, respectively. Their values are list in Table 2.

Table 2 Material properties of 304L solid and powder

Properties	304L Solid	304L Powder
Density, ρ [kg/m^3]	8030	4818
Specific heat capacity, c [J/kg·K]	490	490
Thermal conductivity, k [W/m·K]	16.2	0.269

We solve the above heat transfer equation using the finite difference method. Figure. 5(b) shows the laser heat flux intensity history in a square wave at 0.25 Hz. Figure 5(c) shows the finite difference solution of powder surface temperature for 100 µm powder thickness.

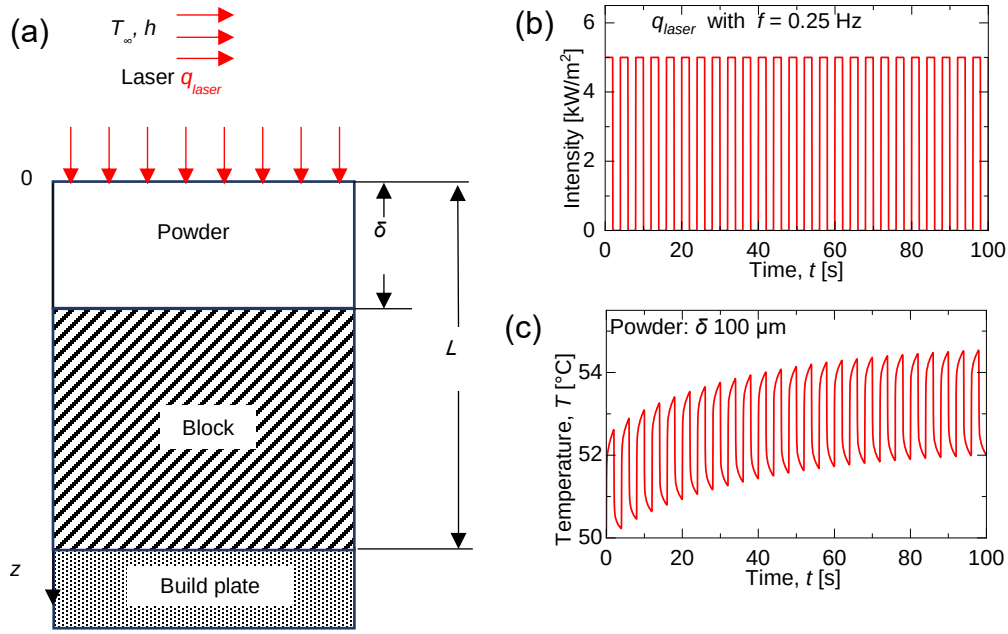

Figure. 5. The 1D heat diffusion model: (a) model definition, (b) laser heating intensity and (c) powder surface temperature response.

Since a square wave can be represented by a Fourier series with infinite terms in frequency domain, the linear heat transfer equation (3) also can be solved in frequency domain. The finite difference solution of the 1D heat transfer equation in frequency domain is shown in Fig. 6 for varying powder thickness. Figure 6(a) shows the phase vs. frequency relationship for different powder thicknesses from 100 µm to 400 µm. The dispersion phases for f_1 = 0.25 Hz are shown in Fig. 6(b), which also has a monotone relationship similar with the experimental result in Fig. 4.

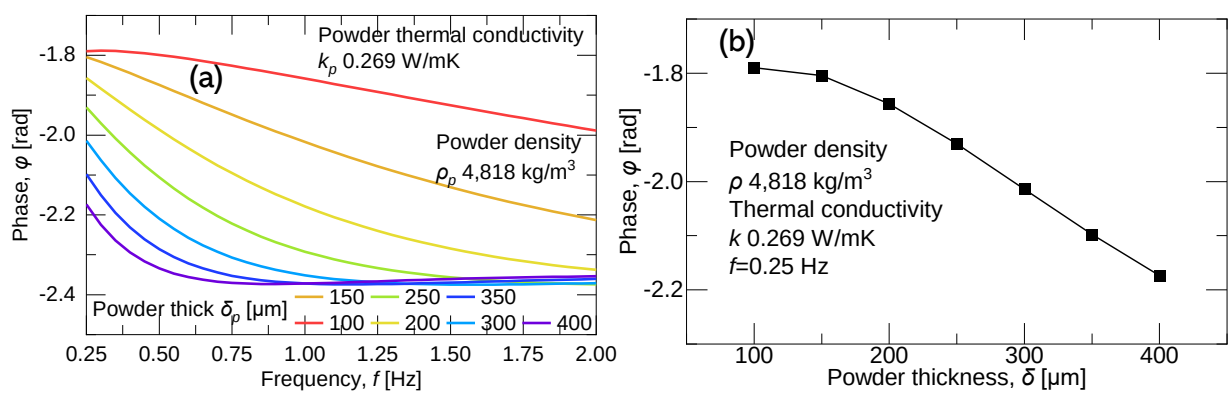

Figure. 6. The finite difference solution of the 1D heat diffusion model in frequency domain with varying powder thickness (a) in frequency domain and (b) for f_1 = 0.25 Hz.

The effect of powder thermal conductivity on the temperature phase is also studied, and the result is shown in Fig. 7(a). This result denotes that all the phase values are dispersive in the frequency range of 0.25-2.00 Hz. At the frequency f_1 = 0.25 Hz, as shown in Fig. 7(b), the monotone relationship between the phase and the powder's thermal conductivity shows the potential for using the phase to monitor in-situ the change in local powder thermal conductivity during the LPBF process.

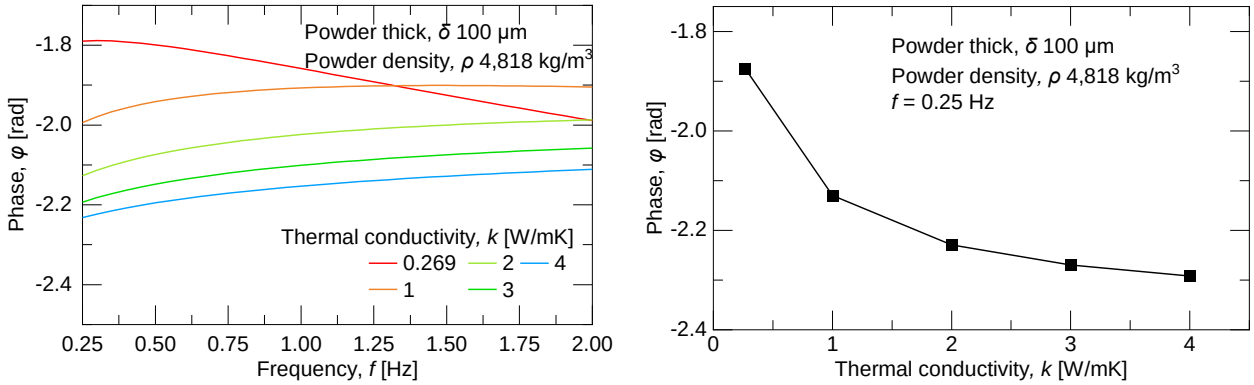

Figure. 7. The finite difference solution of the 1D heat diffusion model in frequency domain with varying powder thermal conductivity (a) in frequency domain and (b) in 0.25 Hz.

It should be noted that the square wave of laser heating results in the surface temperature that can be converted to a Fourier series with infinite terms, with each term corresponding to a different phase. However, the amplitudes of higher-order terms are getting smaller and smaller. Because of their small amplitudes, plus the fact that they may be overwhelmed by the camera noise and powder temperature fluctuations in a real environment, these terms can be ignored in practical implementation.

4. Conclusion

This paper demonstrates the potential of using in-situ active thermography to predict the powder layer thickness and to estimate local powder layer thermal properties during the LPBF process. We have achieved this goal by using an optical diffuser to expand the size of laser beam in a commercial LPBF machine (Renishaw AM 250). A LWIR camera is used to measure the surface temperature resulted from square-wave laser illumination. By analyzing the powder surface temperature history, a monotonic relationship between powder thickness and the phase between surface temperature and laser illumination is obtained at a low fundamental frequency (f_1 = 0.25 Hz). This phase relationship can be used to predict the powder thickness during the LPBF process. The experimentally obtained relationship agrees with the relationship obtained from simulations by solving the 1D heat transfer model numerically in frequency domain. Besides the prediction of powder thickness, the solution of the 1D heat transfer model also demonstrates the potential of using the active thermography with a LWIR camera to monitor change in powder thermal conductivity during the LPBF process.

Our future work will include integrating the active thermography method with a machine learning method for improved predictions. Machine learning could potentially result in better correlations of the phase obtained from the powder surface temperature measurement with powder thickness and also the powder's thermal properties. This is because the large mount of data associated with the large number of Fourier series terms can be incorporated into machine learning without any difficulty.

Reference

1. Constantin, Loic, Nada Kraiem, Zhipeng Wu, Bai Cui, Jean-Luc Battaglia, Christian Garnier, Jean-François Silvain, and Yong Feng Lu. "Manufacturing of complex diamond-based composite structures via laser powder-bed fusion." Additive Manufacturing 40 (2021): 101927.
2. Gould, Benjamin, Sarah Wolff, Niranjan Parab, Cang Zhao, Maria Cinta Lorenzo-Martin, Kamel Fezzaa, Aaron Greco, and Tao Sun. "In situ analysis of laser powder bed fusion using simultaneous high-speed infrared and x-ray imaging." Jom 73, no. 1 (2021): 201-211.
3. Piniard, Matthieu, Beatrice Sorrente, Gilles Hug, and Pascal Picart. "Melt pool monitoring in laser beam melting with two-wavelength holographic imaging." Light: Advanced Manufacturing 3, no. 1 (2022): 1-12.
4. Chen, Hui, Qingsong Wei, Yingjie Zhang, Fan Chen, Yusheng Shi, and Wentao Yan. "Powder-spreading mechanisms in powder-bed-based additive manufacturing: Experiments and computational modeling." Acta Materialia 179 (2019): 158-171.
5. Han, Quanquan, Heng Gu, and Rossitza Setchi. "Discrete element simulation of powder layer thickness in laser additive manufacturing." Powder technology 352 (2019): 91-102.
6. Ma, Mingming, Zemin Wang, Ming Gao, and Xiaoyan Zeng. "Layer thickness dependence of performance in high-power selective laser melting of 1Cr18Ni9Ti stainless steel." Journal of Materials Processing Technology 215 (2015): 142-150.
7. Kempen, Karolien, Evren Yasa, Lore Thijs, J-P. Kruth, and Jan Van Humbeeck. "Microstructure and mechanical properties of Selective Laser Melted 18Ni-300 steel." Physics Procedia 12 (2011): 255-263.
8. Qiu, Chunlei, Chinnapat Panwisawas, Mark Ward, Hector C. Basoalto, Jeffery W. Brooks, and Moataz M. Attallah. "On the role of melt flow into the surface structure and porosity development during selective laser melting." Acta Materialia96 (2015): 72-79.
9. Sufiiarov, V. Sh, A. A. Popovich, E. V. Borisov, I. A. Polozov, D. V. Masaylo, and A. V. Orlov. "The effect of layer thickness at selective laser melting." Procedia engineering 174 (2017): 126-134.
10. Weaver, Jordan S., Justin Whiting, Vipin Tondare, Carlos Beauchamp, Max Peltz, Jared Tarr, Thien Q. Phan, and M. Alkan Donmez. "The effects of particle size distribution on the rheological properties of the powder and the mechanical properties of additively manufactured 17-4 PH stainless steel." Additive Manufacturing 39 (2021): 101851.
11. Wei, Lien Chin, Lili E. Ehrlich, Matthew J. Powell-Palm, Colt Montgomery, Jack Beuth, and Jonathan A. Malen. "Thermal conductivity of metal powders for powder bed additive manufacturing." Additive Manufacturing 21 (2018): 201-208.
12. Abdelrahman, Mostafa, Edward W. Reutzel, Abdalla R. Nassar, and Thomas L. Starr. "Flaw detection in powder bed fusion using optical imaging." Additive Manufacturing 15 (2017): 1-11.
13. DePond, Philip J., Gabe Guss, Sonny Ly, Nicholas P. Calta, Dave Deane, Saad Khairallah, and Manyalibo J. Matthews. "In situ measurements of layer roughness during laser powder bed fusion additive manufacturing using low coherence scanning interferometry." Materials & Design 154 (2018): 347-359.
14. Zhang, Bin, John Ziegert, Faramarz Farahi, and Angela Davies. "In situ surface topography of laser powder bed fusion using fringe projection." Additive Manufacturing 12 (2016): 100-107.

15. Williams, Richard J., Catrin M. Davies, and Paul A. Hooper. "In situ monitoring of the layer height in laser powder bed fusion." Material Design & Processing Communications 3, no. 6 (2021): e173.
16. Alkahari, Mohd Rizal, Tatsuaki Furumoto, Takashi Ueda, Akira Hosokawa, Ryutaro Tanaka, and Mohd Sanusi Abdul Aziz. "Thermal conductivity of metal powder and consolidated material fabricated via selective laser melting." In Key Engineering Materials, vol. 523, pp. 244-249. Trans Tech Publications Ltd, 2012.
17. Pannitz, O., A. Lüddecke, A. Kwade, and J. T. Sehrt. "Investigation of the in situ thermal conductivity and absorption behavior of nanocomposite powder materials in laser powder bed fusion processes." Materials & Design 201 (2021): 109530.
18. Shrestha, Ranjit, and Wontae Kim. "Evaluation of coating thickness by thermal wave imaging: A comparative study of pulsed and lock-in infrared thermography–Part I: Simulation." Infrared Physics & Technology 83 (2017): 124-131.
19. Tomita, Ko, and Michael Yit Lin Chew. "A Review of infrared thermography for delamination detection on infrastructures and buildings." Sensors 22, no. 2 (2022): 423.
20. Moskovchenko, Alexey, Vladimir Vavilov, Michal Švantner, Lukáš Muzika, and Šárka Houdková. "Active IR thermography evaluation of coating thickness by determining apparent thermal effusivity." Materials 13, no. 18 (2020): 4057.
21. Salazar, A., M. Colom, and A. Mendioroz. "Laser-spot step-heating thermography to measure the thermal diffusivity of solids." International Journal of Thermal Sciences 170 (2021): 107124.
22. Hwang, Soonkyu, Yun-Kyu An, Ji-Min Kim, and Hoon Sohn. "Monitoring and instantaneous evaluation of fatigue crack using integrated passive and active laser thermography." Optics and Lasers in Engineering 119 (2019): 9-17.
23. Liu, Tao, Cody S. Lough, Hossein Sehhat, Yi Ming Ren, Panagiotis D. Christofides, Edward C. Kinzel, and Ming C. Leu. "In-situ infrared thermographic inspection for local powder layer thickness measurement in laser powder bed fusion." Additive Manufacturing 55 (2022): 102873.